Large-Scale Structure of the June–July 1996 Marine Boundary Layer along California and Oregon

C. E. DORMAN

Center for Coastal Studies, Scripps Institution of Oceanography, San Diego, California

T. HOLT

Marine Meteorology Division, Naval Research Laboratory, Monterey, California

D. P. ROGERS

Physical Oceanography Research Division, Scripps Institution of Oceanography, San Diego, California

K. EDWARDS

Center for Coastal Studies, Scripps Institution of Oceanography, San Diego, California

(Manuscript received 10 November 1998, in final form 9 August 1999)

ABSTRACT

Data from surface stations, profilers, long-range aircraft surveys, and satellites were used to characterize the large-scale structure of the marine boundary layer off of California and Oregon during June and July 1996. To supplement these observations, June–July 1996 averages of meteorological fields from the U.S. Navy's operational Coupled Ocean–Atmospheric Mesoscale Prediction System (COAMPS) model were generated for the region. Model calculations show a broad band of fast northerly surface winds exceeding 7 m s^{-1} extending along the California–Oregon coast. Buoy-measured peaks of 7.1 m s^{-1} off Bodega Bay, 7.2 m s^{-1} off Point Piedras Blancas, and 8.8 m s^{-1} near Point Conception were reported. Mean winds at the buoys located 15–25 km offshore are generally faster than those at coastal stations, and all station winds are faster in the afternoon.

The aircraft and station observations confirm that an air temperature inversion typically marks the top of the marine boundary layer, which deepens offshore. Along the coast, the marine boundary layer thins between Cape Blanco and Santa Barbara. The inversion base height is at its lowest (195 m) at Bodega Bay in northern California and at its highest at Los Angeles and San Diego (416 m). The inversion strength is strongest between Bodega Bay and Point Piedras Blancas, exceeding 10.8°C. The June–July 1996 marine boundary layer depth from COAMPS shows a gradual deepening with distance offshore.

The model-averaged flow within the marine boundary layer is supercritical (Froude number > 1) in a region between San Francisco and Cape Mendocino that extends offshore to 126.4°W. Smaller isolated supercritical areas occur in the lee of every major cape, with the peak Froude number of 1.3 in the lee of Cape Mendocino. This is consistent with aircraft flights of Coastal Waves '96, when extensive regions of supercritical flow off central California and downwind of major capes were recorded with highest Froude numbers around 1.5–2.0. A broad, wedge-shaped area of nearly critical flow (Froude number > 0.8) extends from Cape Blanco to Point Piedras Blancas and offshore to about 128.5°W in the model output.

The model wind stress has a broad maximum exceeding 0.3 N m^{-2} between Cape Mendocino and San Francisco with the highest values found within 100 km of the coast. Stress calculated directly from low aircraft legs is highest in the lee of large capes with peak values exceeding 0.7 N m^{-2}. Overall aircraft magnitudes are similar to the model's, but a direct comparison with the 2-month average from the model is not possible due to the lesser space and time coverage of the flights. The stress maxima along the California coast shown in the model results are spatially consistent with the region of coldest sea surface temperature observed by satellite.

1. Introduction

The interaction of the lower atmosphere with the Pacific Ocean and the U.S. west coast is the focus of a number of research and problems. Some examples are the atmospheric forcing of the upper ocean through stress and heat fluxes, biological responses to wind-driven coastal upwelling, weather forecasting in the complex coastal zone, and the world carbon cycle (Rotunno et al. 1992; Brink et al. 1992; U.S. GLOBEC 1994). Despite the importance of such problems, representative atmospheric measurements over the open coast are limited.

Corresponding author address: Dr. Clive Dorman, Center for Coastal Studies, Scripps Institution of Oceanography, University of California, San Diego, La Jolla, CA 92093-0209.
E-mail: cdorman@ucsd.edu

Existing large-scale climatologies are based upon ship observations. Nelson (1977) and Nelson and Husby (1983) analyzed ship observations to find that sea level winds accelerate around the North Pacific anticyclone, reaching a broad maximum between Cape Blanco and Point Conception, which extends more than 5° of longitude offshore. Fastest winds are found off of northern California. Based upon a few ship cruises, Neiburger et al. (1961) described the subsidence air temperature inversion at the top of the marine atmospheric boundary layer (MABL) whose base slopes down toward the West Coast, with a minimum height under 400 m and an inversion strength of 10°C between Cape Mendocino and Point Conception. Air begins to subside from 3-km elevation over the Gulf of Alaska. As it sinks over the MABL, it become markedly warmer and drier than air in the MABL, which is cooled and moistened by contact with cold upwelled waters. This three-decade-old study remains the only large-scale description of the air temperature inversion structure over the eastern Pacific, attesting to the difficulties of making atmospheric measurements offshore.

Brief but more detailed snapshots of the MABL have been provided by a limited number of aircraft flights and coastal soundings, mostly near shore (Brost et al. 1982a,b; Beardsley et al. 1987; Bridger et al. 1993; Enriquez and Friehe 1995; Rogers et al. 1998). During the summer of 1981 and 1982, the Coastal Ocean Dynamics Experiment (CODE) conducted over 40 flights near Point Arena, California. CODE captured a shallow air temperature inversion base ($<$50 m) accompanied by high speed surface winds just south of Point Arena (Beardsley et al. 1987), as was found in later observations at Point Sur (Dorman et al. 1999). Such studies have shown a jetlike structure in the winds with the peak centered near the base of the air temperature inversion. The strongest jets are found within 10 of km of the coast.

Several studies have addressed the dynamics of these high speed winds. Zemba and Friehe (1987) attributed the vertical structure of the wind jet to a combination of drag with the sea surface and thermal wind due to horizontal temperature gradients. The horizontal extent of the coastal wind maxima has been investigated numerically by Burk and Thompson (1996), Holt (1996), Cui et al. (1998), and others.

Atmospheric measurements off of the U.S. West Coast are sparse in the extreme. Until recently, there were only two coastal operational upper-air stations that recorded data in the MABL (Rotunno et al. 1992). An anchored weather buoy network of buoys 100–200 km apart and 15–25 km offshore has greatly improved observations within the U.S. west coast zone. Established in the 1980s by the National Buoy Data Center, the buoy network was expanded to a peak coverage in the mid-1990s. The resulting long-term buoy data show two summer coastal speed maxima, one near Point Arena and the other near Point Conception, with speed minima near San Francisco and in the southern California Bight (Halliwell and Allen 1987; Dorman and Winant 1995).

In contrast to the long time coverage of the buoy network, coastal meteorological station observations between Point Conception and Washington have been extremely limited historically. Except for three automated stations, the few operational coastal stations do not typify general MABL conditions and do not exist at all topographically distinct areas along the coast.

An Office of Naval Research field program in the summers of 1994 and 1996 was established to temporarily add enough coastal surface and radar profilers to capture the major alongcoast structure of the MABL. Data from the 1996 program will be discussed in this paper since its coverage extended farther north and it coincided with the Coastal Waves ’96 project. The Coastal Waves ’96 project funded by the National Science Foundation provided extensive NCAR EC-130Q aircraft measurements of the lower atmosphere in June and July 1996 (Rogers et al. 1998). The limited temporal coverage of the aircraft and spatial coverage of the coastal stations was supplemented with June–July 1996 averages of meteorological variables from the U.S. Navy’s Coupled Ocean–Atmospheric Mesoscale Prediction System (COAMPS) model. This ensemble of observations and model results provides an updated description of MABL conditions along the California and southern Oregon coast during summer 1996.

2. Description of measurements and model

a. Stations

The data used in the paper from June and July 1996 were taken during conditions that were consistent with a 10-yr summertime average of West Coast buoy data (Dorman and Winant 1995). To determine near-surface conditions, five different sets of automated meteorological stations were used (Table 1). The National Data Buoy Center (NDBC) maintains buoys located 15–25 km offshore that record wind, pressure, and air and sea temperature hourly (Hamilton 1980). There are 15 buoys between Los Angeles and Newport, Oregon (Fig. 1). The same organization maintains three automated stations on coastline capes that sample wind, pressure, and air temperature.

Scripps Institution of Oceanography installed 15 automated stations between San Diego, California, and Gold Beach, Oregon, as close to the ocean as possible during the summer of 1996. Winds were measured from a 10-m mast. Air temperature and humidity sensors were protected by an aspirated Gill radiation shield. These variables and pressure were recorded as 1-min averages. Since the June–July wind record for 1996 was unavailable at the Scripps Pier in San Diego, data for 1997 were substituted because they were judged to be typical of other summers.

Data from a few existing automated stations are in-

TABLE 1. Surface stations.

Lat (°)	Long (°)	Elev. (m)	SPD (m s^{-1})	Dir (°)	Air temp (°C)	Pressure (hPa)	Operator	Location
44.60	124.50	0	4.1	350	13.4	1018.0	N	B50
44.60	124.10	9	2.8	329	11.7	1017.4-NEWP	N	Newport
43.30	124.40	18	2.3	17	12.1	1017.8-CARD	N	Cape Blanco
42.41	124.42	6	3.0	351	13.6	1017.3-GOLD	S	Gold Beach
41.90	124.40	0	4.2	312	10.9	1015.0	N	B27
41.78	124.25	18	0.9	318	11.9	1016.9	S	Crescent City
40.78	124.25	8	1.4	310	12.2	1017.6-SMOA	S	Somoa
40.40	124.50	0	5.7	359	11.2	1016.4	N	B30
40.03	124.08	12	0.1	342	13.4	1015.0-SHEL	S	Shelter Cove
39.44	123.82	10	1.3	336	11.7	1015.5	S	Fort Bragg
39.20	124.00	0	6.0	325	11.8	1014.3	N	B14
39.13	123.72	46	1.3	292	12.7	1015.8	S	Elk
39.00	123.70	12	4.3	351	11.4	1014.9-ARNA	N	Point Arena
38.76	123.53	15	3.7	314	11.7	1014.7	S	Gualala
38.51	123.25	25	3.0	303	11.7	1014.7	S	Fort Ross
38.32	123.07	9	2.6	317	13.6	1013.1	B	Bodega Bay
38.20	123.30	0	7.1	309	11.3	1014.7	N	B13
37.70	122.80	0	4.9	297	11.6	1013.7	N	B26
37.40	122.70	0	4.1	310	12.1	1013.7	N	B12
37.12	122.32	12	3.4	312	12.9	1015.3	S	Ano Nuevo
36.80	122.40	0	5.2	316	14.8	1014.6	N	B42
36.69	121.76	51	3.9	278	12.9	_____-FORD	P	Fort Ord
36.30	121.89	13	5.8	342	13.0	1014.7-PSUR	S	Point Sur
36.07	121.60	60	0.7	304	12.7	1014.6-BCRK	S	Big Creek
35.70	121.90	0	7.2	312	12.7	1014.9	N	B28
35.67	121.28	7	4.1	326	12.3	1014.4-PPED	S	Point Piedras Blancas
35.26	120.89	12	2.6	349	12.3	—	G	Point Buchon
34.90	120.90	0	5.3	316	12.8	1013.5	N	B11
34.60	120.60	9	8.3	356	—	1013.6	N	Point Arguello
34.50	120.70	0	7.1	319	—	1013.3	N	B51
34.30	120.40	0	8.8	307	13.2	1013.0	N	B54
33.14	119.27	154	6.4	313	17.2	1013.2	U	San Nicolas Is
34.42	119.88	9	0.7	307	16.1	_____-WCAM	A	West Campus
34.20	119.80	0	4.4	283	14.8	1012.3	N	B53
33.80	118.40	0	2.4	320	17.1	1012.1	N	B45
33.70	119.10	0	1.7	282	16.8	1012.3	N	B25
32.87	117.26	9	1.4	275	20.0	1012.5-SIOP	S	Scripps Pier

Operator: N = NDBC, S = Scripps, B = BBML, P + NPGS, G = PGE, U = USN, A = SBAPCD.

cluded. These are from the Diablo Canyon Power Plant maintained by the Pacific Gas and Electric Company, a station near Santa Barbara controlled by the Santa Barbara County Air Pollution Control District, and a station at Bodega Bay operated by the University of California Bodega Bay Marine Laboratory.

Sampling of the lower atmosphere was dominantly by the National Oceanic and Atmospheric Administration/Environmental Research Laboratory's (NOAA/ERL) Environmental Technical Laboratory (ETL) radar profilers (Table 2). Six were between Newport, Oregon, and Goleta (near Santa Barbara). Similar instruments were at Fort Ord, the Los Angeles airport, and on Point Loma in San Diego, which were operated by the Naval Postgraduate School, the South Coast Air Pollution Control District, and the San Diego Air Pollution Control District, respectively. All made hourly averaged wind soundings to above 1.5 km, but varied in the vertical distance over which the data are space averaged. Most of the profilers had Radio Acoustical Sounding Systems (RASSs) to obtain a virtual temperature sounding. Basic data processing for the profilers is discussed in Ralph et al. (1998).

Near some of the NOAA/ERL radar profilers, an additional separate acoustical sounder was operated to capture a temperature sounding of the lower few hundred meters of the atmosphere. Data were also obtained from the Pacific Gas and Electric Company's acoustical sounder on the coast at Diablo Canyon.

b. Aircraft

The National Center for Atmospheric Research's (NCAR) Hercules EC-130Q aircraft was used to survey sections of the California and Oregon coast (Rogers et al. 1998). Eleven flights were made between 2 June and 1 July 1996. Typically, a flight concentrated on a selected topographic area taking 8–10 h for the survey with an airspeed of 100 m s^{-1}. The survey was divided up into legs along which stacks of level runs were flown, including one at 30 m and one at several hundred meters elevation. Repeated vertical profiles through the MABL

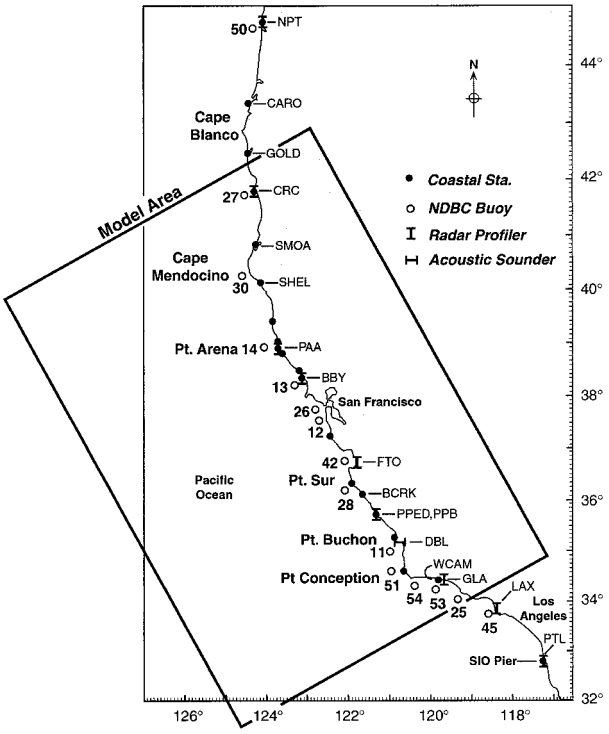

FIG. 1. Station locations and COAMPS model 9-km grid domain.

were flown along each leg. The aircraft measurements included winds, air temperature, humidity, pressure, turbulent fluxes, elevation, and location. The data were sampled at 25 kHz, filtered, processed, and stored in the onboard computer system.

c. Model description

The navy's COAMPS was used to estimate the averaged meteorological scenario for June–July 1996 in order to extend the sparse observations over the west coast. The COAMPS model, which has been verified and tested elsewhere (Hodur et al. 1996; Hodur 1997; Doyle 1997; Thompson et al. 1997; Haack and Hodur 1997; Burk et al. 1999), has been run operationally by the navy in more than five coastal areas of the globe to provide real-time mesoscale forecasts. To substantiate the ability of COAMPS to accurately represent synoptic-scale flow, 12-h forecast root-mean-square (rms) and bias errors of height, temperature, and wind for standard pressure levels from 1000 to 100 hPa verified against radiosondes for COAMPS nest 1 (81 km) for June–July 1996 are shown (Table 3). Though the radiosondes were also used in COAMPS multivariate optimum interpolation (MVOI) analyses, they nonetheless provide an objective measure of COAMPS forecast skill.

The magnitude of height biases decreases from -10 m at 1000 hPa to ~ 0 to -5 m up to 200 hPa. The rms height errors are ~ 25 m at 1000 hPa, decreasing to ~ 14–18 m up to 500 hPa and increasing to ~ 20–35 m at jet level (150–200 hPa). The magnitude of temperature biases are less than -1°C throughout the lower troposphere, with temperature rms errors ~ 3°C at 1000 hPa, decreasing to 1.3°–2.0°C in the midtroposphere. The wind bias at 1000 hPa is approximately zero (0.026 m s^{-1}), with biases on the order of -0.6 to -0.2 m s^{-1} in the midtroposphere (except for 925 hPa, which has substantially fewer wind observations than all other levels). Wind rms errors are less than 3 m s^{-1} below 500 hPa and range from 3.0 to 4.2 m s^{-1} above 500 hPa. The range of these height, temperature, and wind errors are on the order of other COAMPS case studies (see Hodur et al. 1996) as well as errors for the Limited Fine Mesh model and Nested Grid Model models (Junker et al. 1989).

There is no large-scale, high-resolution, long-term dataset that can directly verify the mesoscale structure in the 2-month model averages presented in this paper. However, the success of COAMPS in previous case studies, in comparison with Coastal Waves '96 aircraft data (section 5a), and in indirect comparison with available large-scale observations (section 6), justifies the use of the COAMPS output to estimate mean conditions during this period.

TABLE 2. Sounding stations and inversion characteristics.

Station	Lat (°)	Long (°)	Elev. (m)	Inv. base ht (m)	Inv. top ht (m)	Inv. base temp (°C)	Inv. top temp (°C)	Inv. strength (°C)	% Occur	Type	Oper-ator	Location
NPT	44.58	121.06	40	319	738	14.2	21.3	7.0	34	R	N	Newport
CRC	41.78	124.24	15	218	797	12.7	21.5	8.8	67	R	N	Crescent City
PAA	36.95	122.07	18	251	622	12.3	22.2	9.9	63	R, A	N	Point Arena
BBY	38.32	123.07	12	195	732	13.4	24.6	11.2	94	R	N	Bodega Bay
FTO	36.69	121.76	51	336	916	13.2	24.1	10.8	90	R	P	Fort Ord
PPB	35.67	121.28	11	256	789	14.0	25.2	11.2	82	R	N	Point Piedras Blancas
DBL	35.20	120.84	61	282	—	—	—	—	—	S	G	Diablo Canyon
GLA	34.43	119.06	3	235	937	17.3	25.6	8.3	85	R	N	Goleta
LAX	33.94	119.41	47	417	1004	17.2	25.0	7.8	91	R	S	Los Angeles
PTL	32.41	117.15	23	416	824	17.1	24.9	7.8	92	R	D	Point Loma

Type: R = radar profiler with RASS; A = acoustical sounder; S = SODAR.
Operator: N = NOAA ERL; P = NPGS; G = PGE; S = SCAPCD; D = SDAPCD.

TABLE 3. COAMPS 81-km statistics for Jun–Jul 1996.

Level (Mb)	No. of obs	Bias
Heights verified against raobs		
100	4746	−20.560
150	4808	−8.005
200	4838	−3.742
250	4863	−4.451
300	4891	−4.618
400	4930	−4.898
500	4940	−3.679
700	4944	−0.334
850	4948	−1.434
925	4166	−2.301
1000	5002	−10.792
Temperatures verified against raobs		
100	4735	0.247
150	4807	−0.254
200	4837	−0.117
250	4858	0.142
300	4890	0.186
400	4930	−0.006
500	4935	−0.333
700	4941	−0.696
850	4366	−0.057
925	492	−0.439
1000	1077	−0.791
Winds verified against raobs		
100	4544	1.268
150	4642	0.305
200	4642	−0.238
250	4662	−0.206
300	4709	−0.003
400	4847	−0.189
500	4837	−0.426
700	4758	−0.589
850	3982	−0.167
925	72	−1.159
1000	1015	0.026

TABLE 4. Model level heights (m).

31 050	12 425	7800	2300	215
24 400	11 675	6800	1600	140
19 400	10 925	5800	1100	90
16 050	10 175	4800	750	55
14 300	9425	3900	500	30
13 300	8675	3100	330	10

The remainder of this section describes the model setup. The atmospheric portion of COAMPS was used. The nonhydrostatic, fully compressible equations of motion are solved in three dimensions on a terrain-following sigma-*z* coordinate system (Gal-Chen and Somerville 1975). Parameterizations of physical processes in COAMPS include short- and longwave radiation (Harshvardhan et al. 1987), convection (Kain and Fritsch 1990), and subgrid-scale boundary layer processes using a level-2.5 turbulent kinetic energy (TKE) scheme (Therry and LaCarrere 1983). Explicit moist physics is included through prognostic equations of cloud water, cloud ice, raindrops, snowflakes, and water vapor (Rutledge and Hobbs 1983).

The COAMPS forecasts produced in support of the field program were run on the Fleet Numerical Meteorology and Oceanography Center (FNMOC) Cray C90. The model simulated data every 12 h. Beginning in late May 1996, the model was cold started using the navy's global spectral model NOGAPS (Navy Operational Global Atmospheric Prediction System) fields interpolated to the COAMPS domain for a first guess. Subsequent forecasts throughout June and July used COAMPS 12-h-old forecasts as first guess fields for the MVOI analysis scheme on each nest, except for two periods when cold starts were required due to database problems. Data used in the analysis step included winds from radiosondes, pibals, aircraft reports, Aircraft Communications and Reporting System, Special Sensor Microwave/Imager (SSM/I), surface stations (including NDBC fixed buoys), and cloud tracks winds. Height/thickness observations were obtained from radiosondes, and Defense Meteorological Satellite Program and NOAA satellites. None of the Coastal Waves '96 aircraft, the radar profilers (Table 2), or surface land station data was used in the first guess fields or the COAMPS analysis. Quality control algorithms developed by Baker (1992) were used to select high quality, representative data. Lateral boundary conditions at 3-h intervals were provided by NOGAPS forecasts. The model topography is derived from the Defense Mapping Agency's 100-m resolution dataset subsampled to 1-km resolution. Sea surface temperature (SST) is obtained by a bilinear interpolation of the FNMOC global 1° SST optimum interpolation analysis to the COAMPS domain. This analysis captures the major features of the coastal upwelling SST pattern.

The configuration of the model was triply nested with one-way interaction between the coarse-mesh domain 61 × 61 grid points, the medium-mesh 61 × 67 grid points, and the fine-mesh 79 × 109 grid points centered over the central California coast. The horizontal resolution was 81 km, 27 km, and 9 km for the three grids, respectively, with the domain of the latter shown in Fig. 1. The model top was at 30 km with 30 vertical levels irregularly spaced, and 11 levels in the lowest 1600 m, down to 10 m (Table 4). The Kain–Fritsch convection parameterization was used only on nests 1 and 2 (81 km, 27 km) while nest 3 (9 km) used the Rutledge and Hobbs explicit moist physics. See Hodur (1997) for a more in-depth description of COAMPS model details.

COAMPS fine-mesh analyses every 12 h were used to create the domain-averaged plots presented in section 4 using standard statistical measures. Because of database problems on the FNMOC Cray C90 unrelated to COAMPS, real-time runs were not made for the following three time periods: 1200 UTC 29 June to 0000 UTC 30 June, 0000 UTC 4 July to 1200 UTC 4 July, and 1200 UTC 9 July to 0000 UTC 13 July. Data for these time periods are not used in computing the statistics. The 2-m air temperature was computed from the

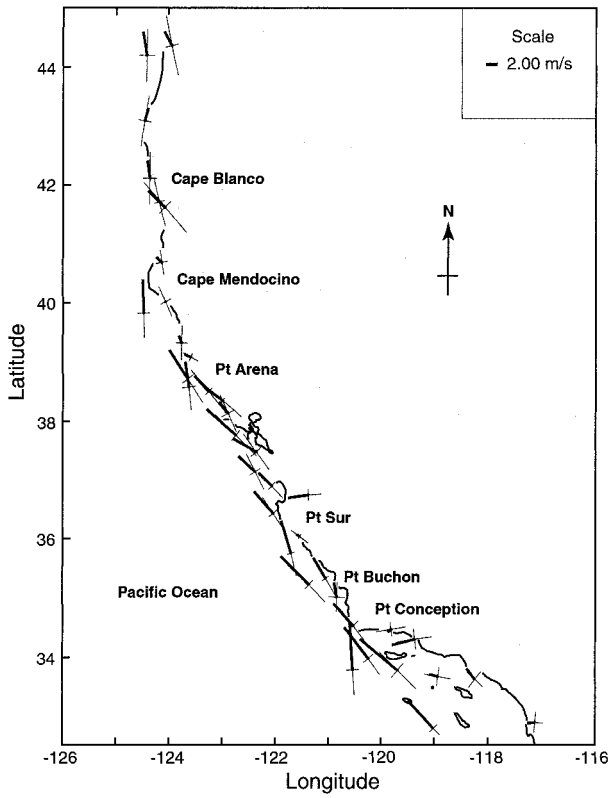

FIG. 2. Automated surface station mean speed and principle axis of winds for Jun–Jul 1996. Mean is the vector with a cross on the downwind end. The cross at the end of the wind vector is the wind standard deviation with the long side the maximum magnitude and orientation and the short side the minimum.

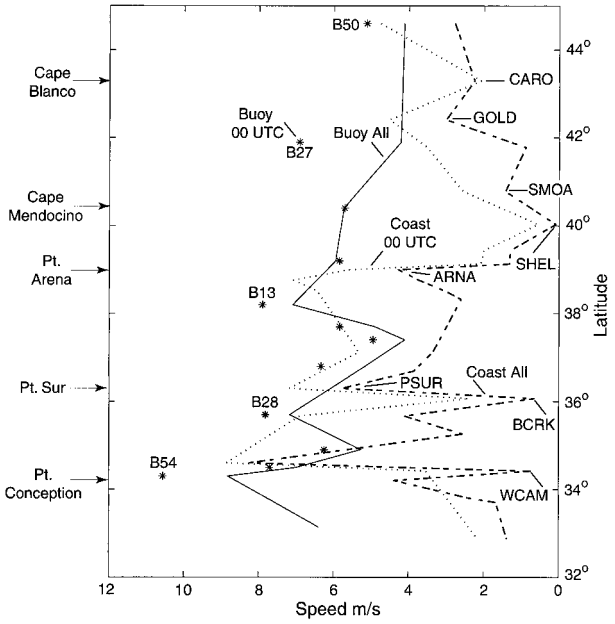

FIG. 3. Daily averaged wind speeds vs latitude for stations in Fig. 2. The left line represents offshore stations, and the right line represents coastal stations. The values at 1600 PST are shown for the offshore stations (asterisk) and coastal stations (dotted line), which is near the time of the diurnal speed maximum.

lowest model-level potential temperature (10 m) and surface layer similarity theory. Wind stress was computed using the surface layer parameterization of Louis et al. (1982).

3. Measurements

a. Surface stations

Buoy data show that northerly surface winds extend from midway along the Oregon coast to south of Point Conception, California, in summer (Fig. 2). The fastest wind speeds are found between Cape Mendocino and Point Conception. Most buoy winds align with the local coast, but there are exceptions due to topographic irregularities. The most significant are the regions of cross coast flow at Newport, Fort Ord, Ventura/Oxnard, and San Diego, which have relatively broad low coastal plains inland. The MABL flow splits past Point Arguello/Point Conception, with most flow continuing to the south-southeast out over open water and some turning into the Santa Barbara Channel. Farther to the southeast of Point Conception, the flow is quite weak in the Southern California Bight (Dorman 1982; Dorman and Winant 1995).

To show the trends in the MABL with distance along the coast, wind speeds averaged over June and July 1996 are plotted versus latitude in Fig. 3. The stations fall into two groups: buoys and land stations. Winds at the buoy stations are faster than the nearest land station in all cases except at Point Arguello. The buoy wind values are high from Cape Mendocino (B30) to Bodega Bay (B13), with a maximum at the latter. A second peak extends from Point Sur to past Point Conception, with the highest overall values at B54, which is at the western mouth of the Santa Barbara Channel. These two broad peaks are separated by a minimum speeds at B26 and B12, which may be related to the gap in the coastal mountains around San Francisco (see Fig. 1). Both broad peaks are asymmetrical alongshore, with the maximums displaced to the south.

The mean land station speeds decrease from central Oregon to Shelter Cove on the south side of Cape Mendocino. Farther south, wind speeds are irregular with local maxima found between Point Arena and Point Conception and the fastest winds at Point Sur and Point Arguello. Weakest mean speeds are at Shelter Cove, Big Creek, and West Campus, which are all in the lee of major topographic points. For reference, land station and buoy speeds at 1600 Pacific standard time (PST), typically the time of the afternoon wind maximum, are plotted in Fig. 3. For all but the coastal station near Cape Blanco (CARO), the 1600 PST speed is greater than the mean speed averaged over the day, with land stations showing the greatest contrast. The land station's

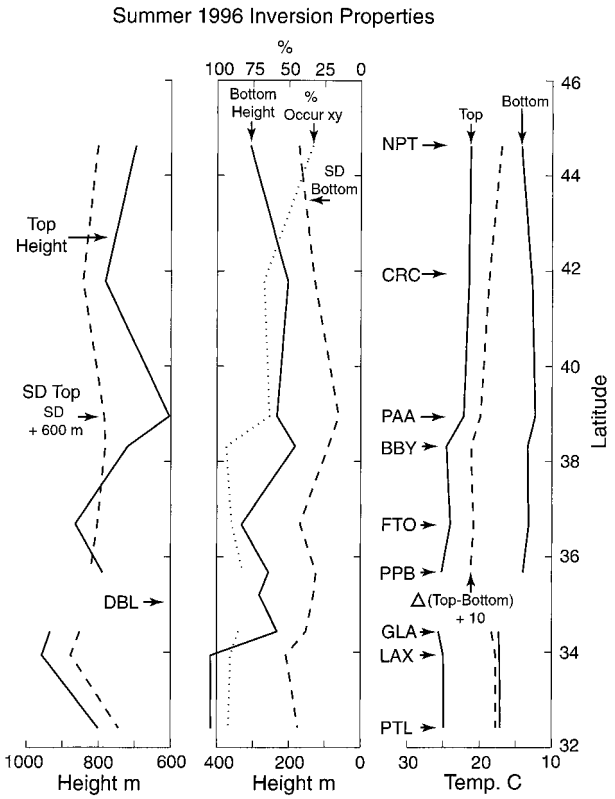

FIG. 4. Inversion properties. (left) Inversion top height (solid) and standard deviation + 600 m (dashed). (middle) Inversion base height (solid), standard deviation (dashed), and percent occurrence of inversion (dotted). (right) Air temperature of the inversion top (solid, left), air temperature of the inversion base (solid, right), temperature difference top minus base +10°C (dashed).

1600 PST value is everywhere less than that of the nearest buoy.

It should be pointed out that the standard deviations of the wind speeds are in the range of 3–4 m s^{-1} for the 2-month period. Nevertheless, an examination of individual station records from the coastal 6-month time series, as well as decade-long buoy records (Dorman and Winant 1995), supports the conclusions drawn above.

b. Upper-air stations

Data collected from a coastal network of 10 profiling stations that measured the lower 1–2 km of the atmosphere between Newport, Oregon, and San Diego are used to characterize the MABL properties for June and July of 1996 (Fig. 4, Table 2). The base of the air temperature inversion decreases from Newport, Oregon, to a minimum of 183 m at Bodega Bay (middle frame). Farther to the south, it rises weakly along the central California coast before dipping to a local minimum at Goleta in the Santa Barbara Channel. The highest bases (>400 m) are found in the Los Angeles–San Diego area. Lower inversion bases along the mid-California coast are associated with generally faster buoy and land station winds.

The percent of occurrence of the inversion base is greatest in the southern portion between Bodega Bay and San Diego (>80% of the time), less often in the northern California section between Point Arena and Crescent City (about 65%) and least often along the central Oregon coast (34%). The presence of the inversion may be underrepresented in the northern California section, since the inversion base height cannot be measured if it is lower than the altitude at which the lowest data can be measured, about 250 m above sea level for those stations. Profiles that showed no inversion were not included in the 2-month averages. The less persistent and lower inversion base to the north is consistent with midlevel synoptic features crossing the coast north of Cape Mendocino. These synoptic systems can eliminate the inversion by switching from subsidence to lifting. Even if the centers of these traveling synoptic features cross the Oregon coast, the southern portion can still disrupt the inversion along the northern California coast. These features are infrequent or very weak south of Point Arena.

The alongcoast structure of the top of the inversion differs from that of the bottom (Fig. 4, left frame). The top height decreases from central Oregon to an absolute minimum at Point Arena and rises to its highest elevation in the southern California Bight at GLA and LAX. The warmest top is found along central California at PPB and GLA. However, the strength of the inversion (top minus base temperature) is greatest, about 11°C, along the mid-California coast between BBY and PPB. The warmer base temperatures sets the southern California Bight off from the rest of the coast.

The temperature of the MABL is influenced by its contact with the sea surface. Coastal sea surface temperatures are coolest along central California, which is concurrent with the coolest MABL inversion base air temperature, as will be discussed later. The warmest air temperatures are in the southern California Bight where the sea surface is the warmest (Robinson 1976; Dorman and Winant 1995).

c. Aircraft

The NCAR EC-130Q aircraft made 11 flights along the coast in the summer of 1996 that provide the first measurements of the MABL in several locations as well as a reference for the land measurements and for the COAMPS model. A flight in the vicinity of each of four major topographic features during strong northerly winds is presented here. Strong wind conditions were selected because the COAMPS June–July 1996 average suggests such conditions were typical; also, it was desirable to compare the structure in the MABL under similar conditions at different sites. Although the number of flights is not sufficient to generate a 2-month average of the MABL, each flight showed the strong

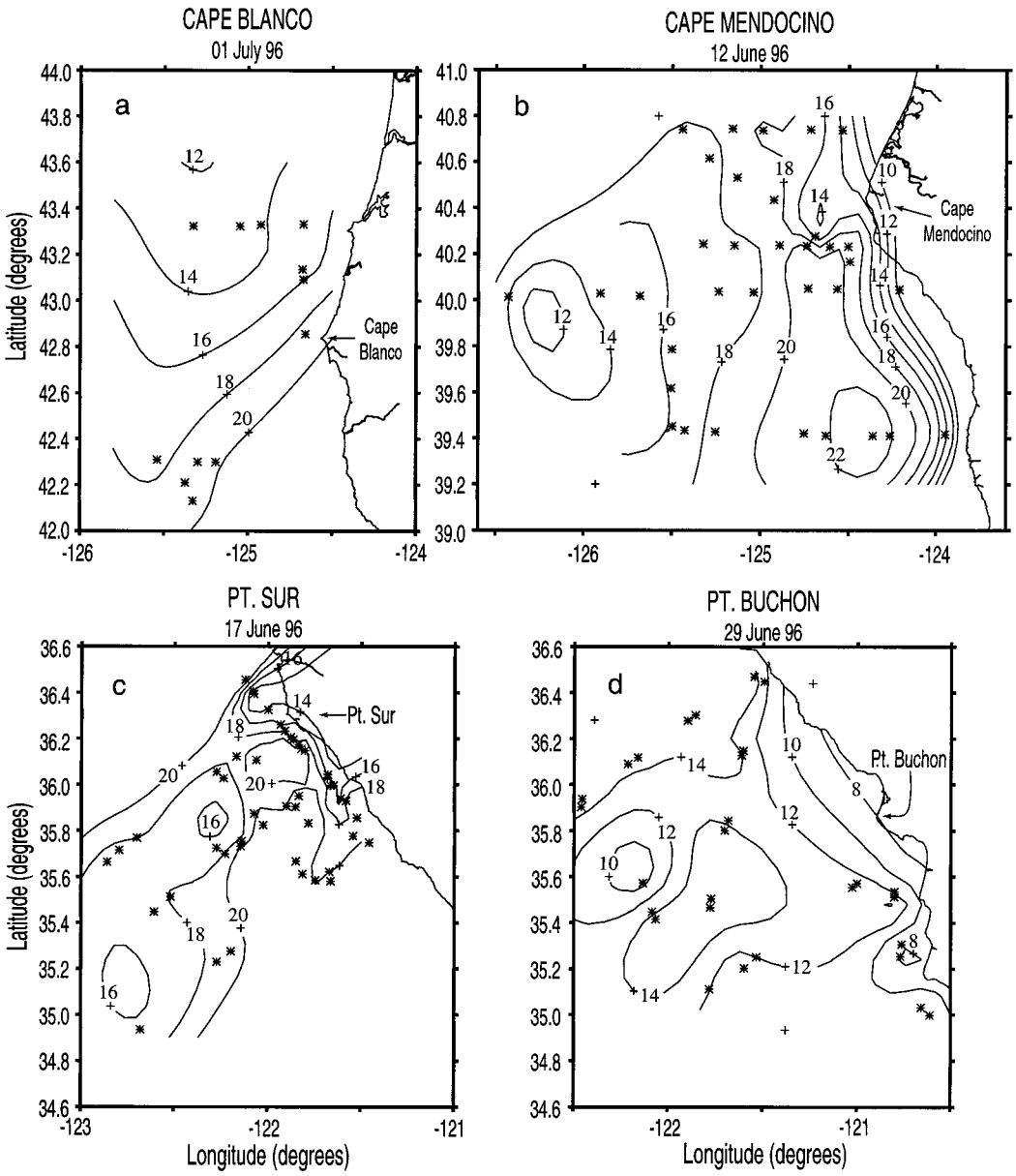

FIG. 5. Aircraft-measured winds adjusted to 10 m at four locations in 1996.

variability in the MABL near topography. Each flight took about 7 or 8 h to complete, but conditions are assumed to be stationary during the flight period, an assumption supported by examination of the nearest buoy and coastal stations (an example is shown in Dorman et al. 2000). In Figs. 5–7, the sounding locations used to generate each map are marked with an asterisk. When interpreting the maps the reader must assume that structure in the mapped fields is less reliable where the sampling was sparse. Where the sampling is more dense, the variability in the MABL over short spatial scales is evident, as seen in other studies (Winant et al. 1988; Enriquez and Friehe 1995). Despite sampling limitations, the aircraft observations represent a significant increase in the record of the MABL in the region.

Wind speeds measured by the aircraft at 30 m when making soundings were reduced to 10 m by assuming the log-wind law and neutral stability (described in Dorman et al. 1999). For Cape Blanco, Cape Mendocino, and Point Sur (Fig. 5), the 10-m wind speeds increase from the 12–16 m s^{-1} range on the upwind side of the cape to more than 20 m s^{-1} downwind, decreasing offshore to 12–14 m s^{-1}. Enriquez and Friehe (1995) found similar structure in the wind field around a topographic point using CODE data. A small minimum wind speed area is found on the north side of Point Sur near the

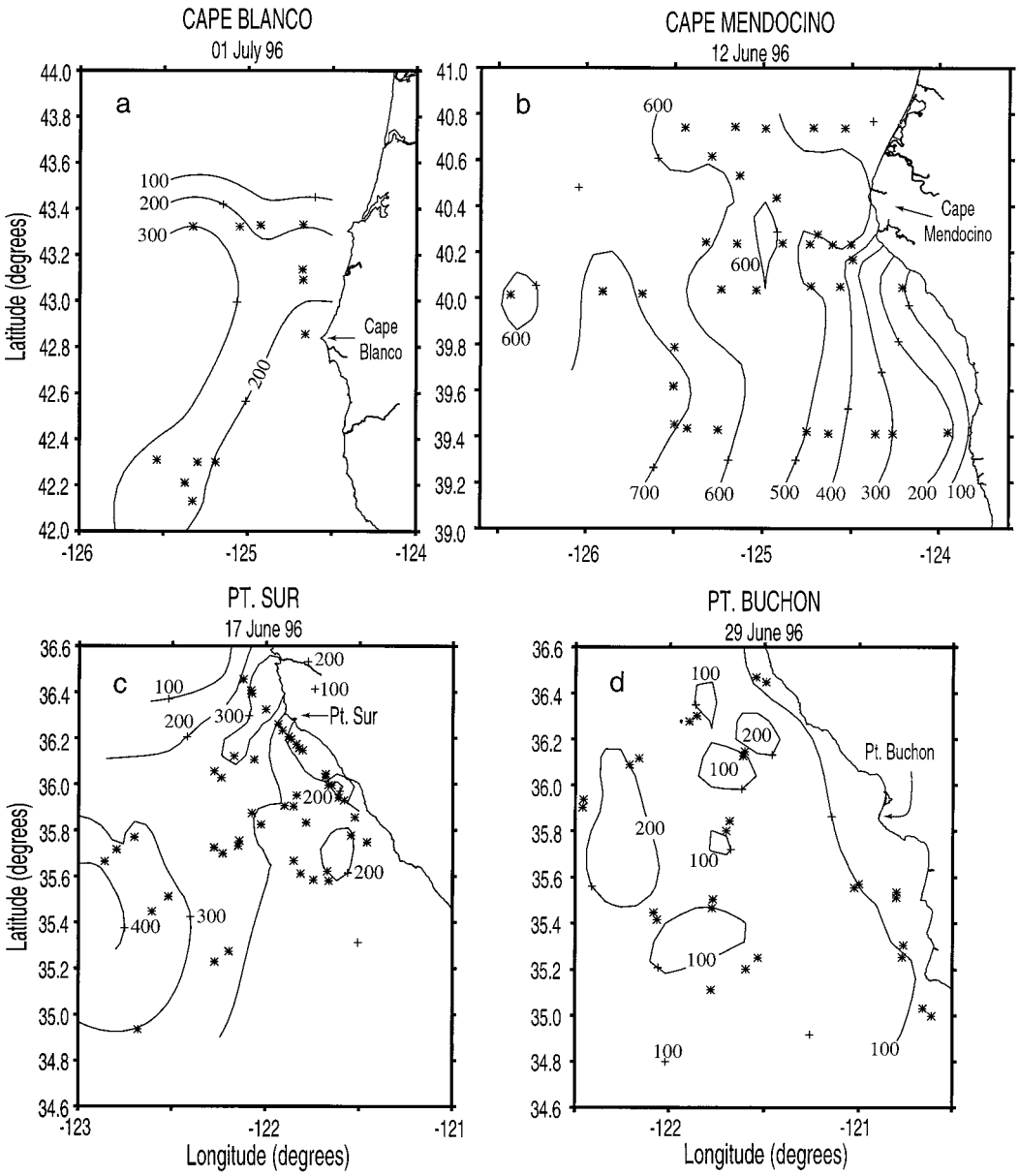

FIG. 6. Aircraft-measured inversion base heights at four locations in 1996.

coast, while there is an extensive weak wind area over the coast on the north side of Point Conception.

The air temperature inversion base height (Fig. 6) was identified from the aircraft soundings as a sharp increase in the gradient of temperature with altitude. The inversion base height near the coast is typically higher on the upwind side of major topographic points and lower on the downwind side. This is most evident for Cape Mendocino and Point Sur. Observations near Cape Blanco were curtailed by an engine problem. For all areas the inversion base height increases with distance offshore to 300–600 m.

As in Dorman et al. (1999), the shallow-layer Froude number of the MABL is calculated from the aircraft soundings by

$$\mathrm{Fr} = \frac{V}{\sqrt{gH\dfrac{\theta_u - \theta}{\theta}}},$$

where g is the acceleration of gravity, H is the height of the mean elevation between the inversion base and top, θ is the potential temperature of the air temperature inversion base, θ_u is the potential temperature of the air temperature inversion top, and V is the mean speed from the sea surface to H. It should be noted that the resulting

Froude number will be smaller than a Froude number that uses the height of the inversion base as the MABL height. While a two-layer Froude number is an idealization of the real, continuously stratified MABL, it has been successfully applied to the inversion-topped MABL in many studies (e.g., Winant et al. 1988; Samelson 1992; Rogers et al. 1998). Burk et al. (1999) found that major features of a continuously stratified simulation of the flow around Cape Mendocino correspond to those found in shallow-water flow. Since the inversion strength is typically 10° or more, a shallow-water Froude number is appropriate for capturing overall features of the flow, such as those presented in this analysis.

The Froude number increases for a shallow-water layer or faster wind speeds. A layer with a Froude number greater than one is supercritical and is associated with special dynamics, as is discussed in classic open channel flow texts (Henderson 1966). Major features such as expansion fans and hydraulic jumps have been identified in the supercritical MABL (Winant et al. 1988; Samelson 1992). An initially subcritical MABL with a Froude number in the range >0.5 but <1 was shown to accelerate to supercritical, undergoing an expansion fan at realistic coastline bends (Rogerson 1999). An example of subcritical upstream flow that produces an expansion fan in the supercritical lee was found at Point Conception (Dorman and Winant 2000).

Aircraft profiles were used to generate Froude number maps presented in Fig. 7. The Cape Blanco flight shows supercritical MABL flow for approximately 40–50 km offshore. The Cape Mendocino flight shows a supercritical region 70–100 km offshore on the south side of Cape Mendocino with a subcritical region along the inner coast on the north side of Cape Mendocino. The MABL flow around Point Sur is almost entirely supercritical with the supercritical flow extending to the edge of the 120-km-wide survey region. West of Point Buchon, there is a broad zone of supercritical flow between subcritical flow in the distant offshore and in the inner coastal zone.

The cases presented for Cape Blanco, Cape Mendocino, and Point Sur resemble supercritical MABL flow accelerating and thinning within an expansion fan in the lee of a cape by Samelson (1992). Using aircraft observations, Winant et al. (1988) found that the acceleration and thinning observed downstream from Point Arena matched a simple analytical solution for a supercritical expansion fan. Similar observations (Dorman et al. 1999) for Point Sur and aircraft data taken around the Capes Blanco and Mendocino (unpublished) also support this hypothesis. On the upwind side of all of these topographic features, the MABL is slower and thicker than on the downwind side, which is also noted in Samelson (1992).

4. Model results

To show large-scale features beyond the scope of the aircraft surveys, 9-km COAMPS output at 0000 and 1200 UTC were averaged for June and July 1996. The COAMPS model domain was extended in both the meridional and zonal directions to capture the region of enhanced nearshore winds. The COAMPS 10-m wind field contains a broad maximum of speeds greater than 7 m s^{-1} extending from Cape Mendocino to past Point Conception (Fig. 8a). The absolute maxima (>9 m s^{-1}) occurs in the southern portion, approximately 100 km offshore from Point Conception. However, there are small speed peaks in the immediate lee of Cape Mendocino and Points Arena, Sur, and Conception. A broad weaker wind zone extends along the coast from San Francisco to the north edge of Point Sur, from Point Piedras Blancas to the north side of Point Conception, and in the eastern portion of the Santa Barbara Channel.

Contours of average sea level pressure run meridionally in the area west of 126°W (the model plots are tilted off of a north–south line). To the east of 126°W, and south of Cape Mendocino, the isobars tend to follow the coast (Fig. 8b). The most extreme bend in the isobars is where they turn sharply east following the coast around Point Conception and into the Santa Barbara Channel. Interestingly, the reduction of the pressure gradient to the south between Cape Mendocino and Point Conception does not correlate with a reduction in the general wind speeds in this area. This is consistent with the National Weather Service three-hourly pressure analysis in this area, in which the alongshore pressure gradients are often poor indicators of the buoy wind speeds.

The 2-m air temperature has a broad minimum of air cooler than 12°C that extends southward from Oregon and ends just north of Point Conception (Fig. 8c). In a narrow, inner coastal zone, an air temperature minimum of less than 11°C extends from Cape Mendocino to Point Piedras Blancas. The model sea surface temperature is about 1°C warmer than the 2-m air temperature and follows the same trends.

An estimate of the depth of the MABL from the model using the same method as from the aircraft data yielded depths that were generally much shallower than observed. This is due to fact that slightly stable boundary layers are often simulated in the model very near the ocean surface. However, a more accurate representation of the depth of the mixing in the lower part of the atmosphere is determined by the model TKE. An estimate of the mode 1 MABL depth was determined by a vertical scan upward from the lowest mode 1 sigma level until TKE exceeded a critical value taken as 1.0×10^{-4} m^{-2} s^{-2}. This determination is purely empirical and is used only for output purposes, not in the internal dynamics of the model. The June–July 1996 model depth using this method is shown in Fig. 8d. Lower MABL depths are found close to the coast, with the shallowest (<400 m) in the lee of capes. The MABL depth increases to the west, approaching 800 m at the extreme southwestern edge of the model boundary. These heights are consistent with the June–July 1996 aircraft

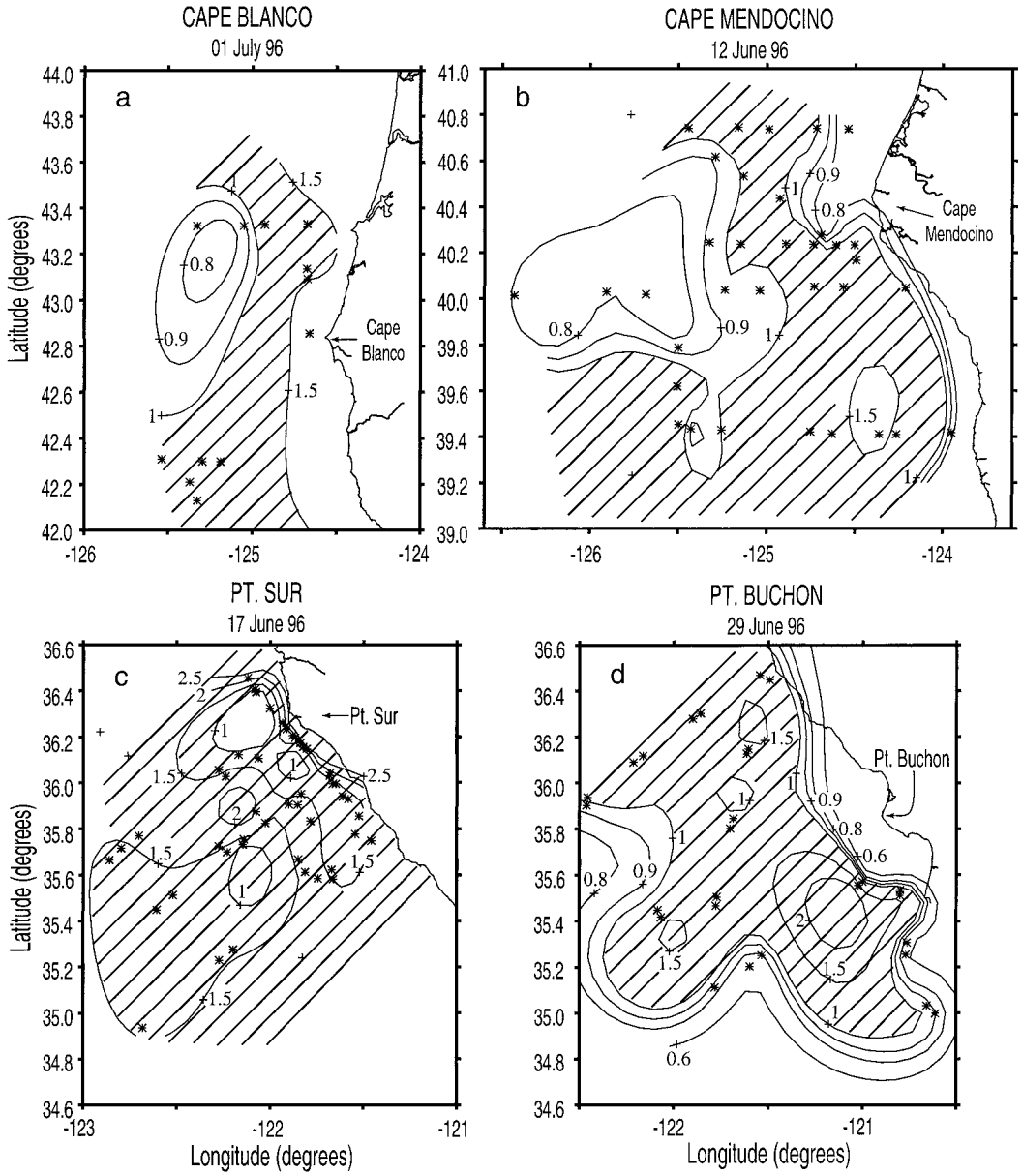

FIG. 7. Froude numbers at four locations in 1996 based upon aircraft profiles.

measured heights in areas offshore of about 80–100 km off the coast. More distant offshore values are consistent with earlier but limited aircraft measurements (Brost et al. 1982) as well as the classical Neiburger et al. (1961) analysis.

To represent the fields that may be impacting the MABL from above, the 925-hPa surface was used since its altitude is near the top of the air temperature inversion and above the MABL. The 925-hPa height field, which can be taken as a measure of the large-scale pressure forcing imposed on the MABL from above, follows the same trends as the sea level pressure, namely lower toward the coast and to the south (Fig. 9b).

Winds on the 925-hPa surface are northerly, with a single, broad peak that exceeds 12 m s^{-1} (Fig. 9a). The eastern edge of the wind maximum laps over Cape Mendocino. The separation between the 10 m s^{-1} isotach and the coastline increases with distance to the south, resulting in weaker coastal winds further to the south.

Air temperature on the 925-hPa surface increases toward the coast and to the south (Fig. 9c). It rises from 18°C over Cape Mendocino to 24°C at Point Conception. In addition, there are isolated structures over the coast that are presumably related to the local topography.

The standard deviation of the air temperature on the 925-hPa surface (Fig. 9d) can be used to assess how the variability in the air temperature inversion changes

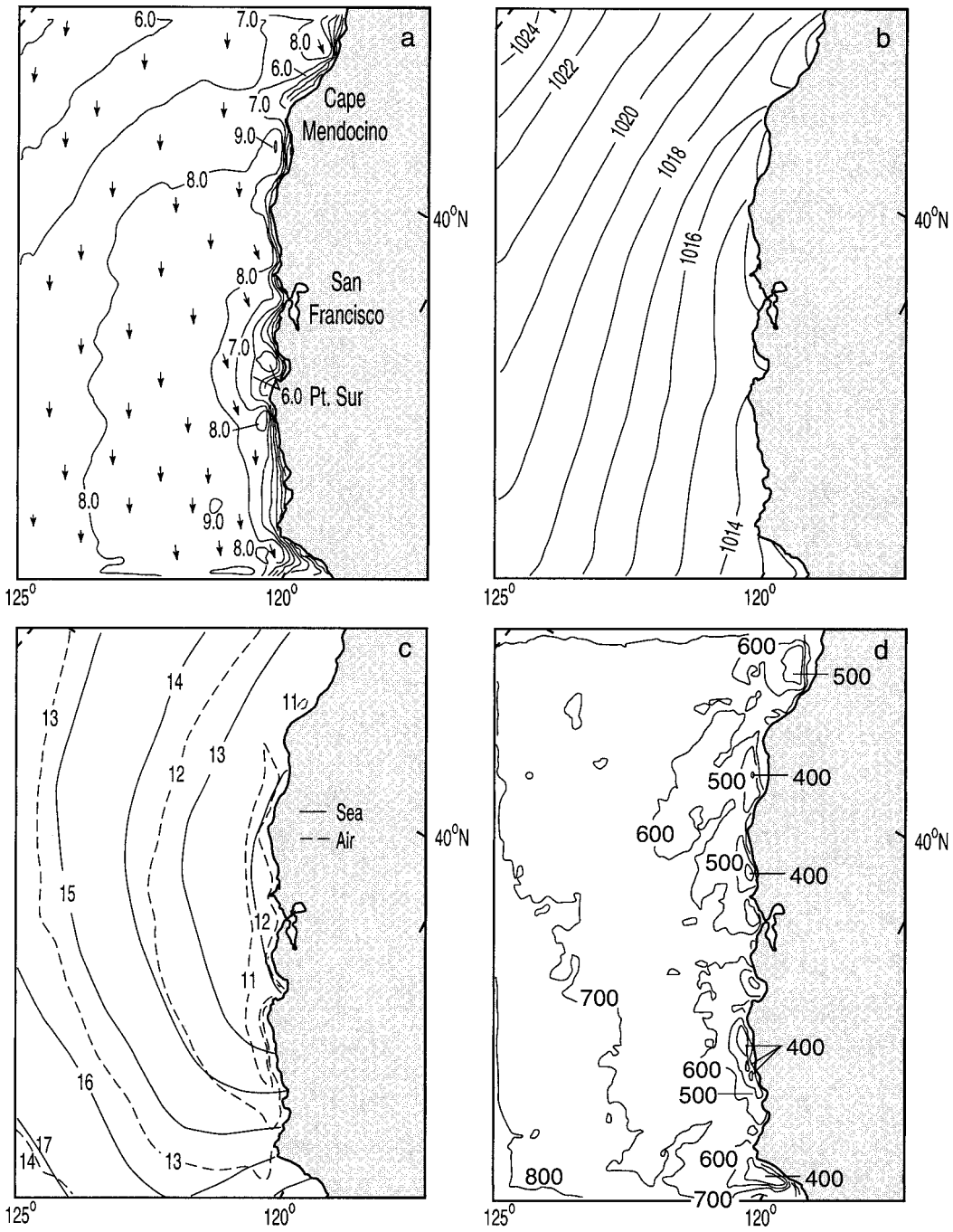

FIG. 8. The 10-m wind speeds (m s^{-1}) and vectors for the COAMPS 9-km grid (upper left) sea level pressure (hPa) (upper right), sea and 2-m air temperature (°C) (lower left), and MABL depth (m) (lower right).

with position. The variability over the ocean is greatest adjacent to southern Oregon and northern California, reflecting the tendency of weak summer traveling cyclones and anticyclones to pass north of Cape Mendocino (Petterssen 1956). In addition, the variability is greatest at the coast, reflecting weak synoptic-scale and midlevel features that move downcoast as they to circle around the east side of the northeast Pacific anticyclone.

The model-derived Froude number is computed using (1) of section 3c with boundary layer depth H determined by the TKE profile (Fig. 8d). A large supercritical area extends between about northern Monterey Bay and 40°N in the model average (Fig. 10a). Peaks of Froude number greater than 1.2 extend from the lee of Cape Mendocino to northern Monterey Bay. Smaller isolated supercritical areas are in the lee of Cape Blanco, around

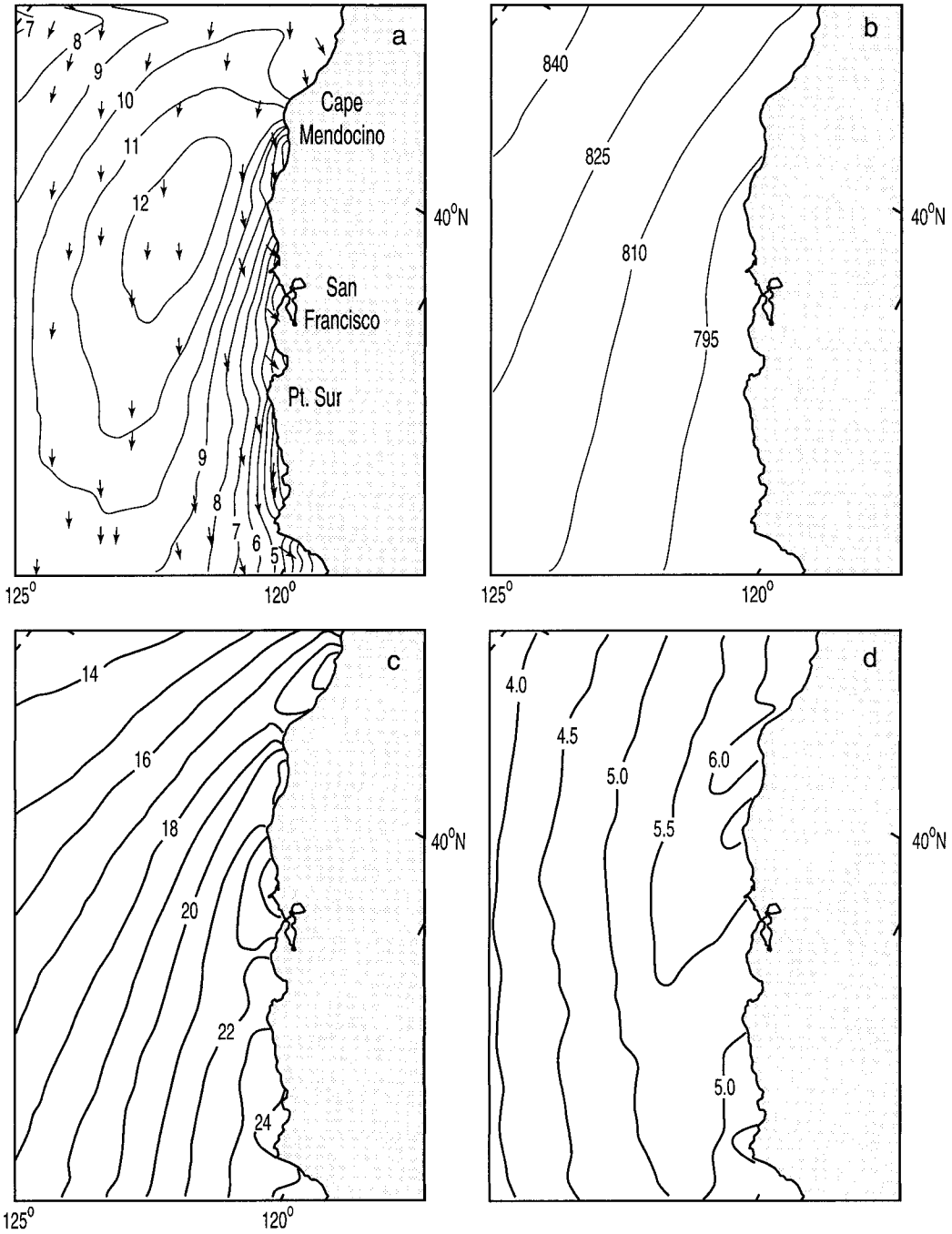

FIG. 9. (a) The 925-hPa wind speed (m s^{-1}) and vectors, (b), 925-hPa geopotential height (m), (c) 925-hPa air temperature (°C), and (d) standard deviation (°C).

Point Sur, and in the Santa Barbara Channel. Froude number maxima in the lee of capes in the COAMPS average are consistent with the June–July 1996 aircraft measurements shown in Fig. 7 and reported in Dorman et al. (1999), Dorman and Winant (2000), and Rogers et al. (1998).

Almost all of the California coast north of Point Conception and beyond 150–300 km offshore has a Froude number greater than 0.8, which would be consistent with supercritical flow during part of the averaging period. Even if not supercritical, transcritical conditions (Fr close to 1) should be common in the lee of topographical points in this area.

The standard deviation of the Froude number is shown in Fig. 10b. A contiguous area with maximum values occurs next to the coast from southern Oregon

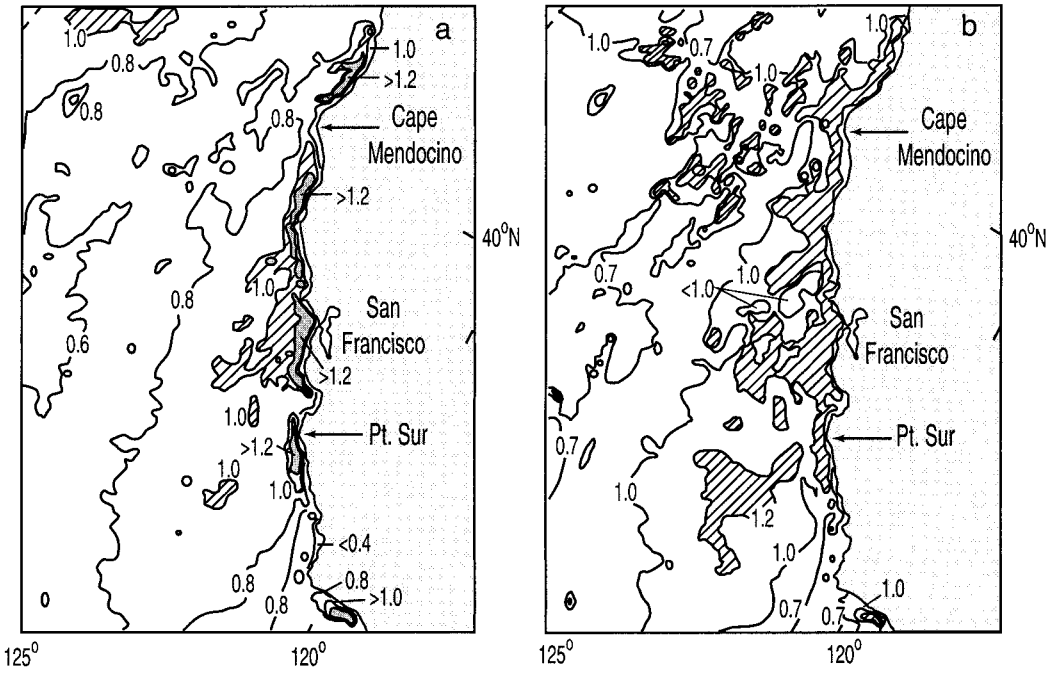

FIG. 10. (a) MABL Froude number and (b) standard deviation. Areas with the Froude number greater than 1.0 are hatched and greater than 1.2 are solid.

to central California. Higher values text to extend downwind and offshore of capes.

5. Sea surface wind stress

a. Aircraft flux measurements

Direct measurements of sea level stress over an area is rare. Usually, there are only spot buoy measurements from which the stress is inferred using bulk methods (Enriquez and Friehe 1997). Enriquez and Friehe (1995) presented one of the first California coastal stress maps based upon aircraft observations. More recently, the Coastal Waves' 96 project collected 25-kHz data at 30-m elevation along horizontal legs from which the stress can be directly calculated, in some regions for the first time. Stresses were calculated by the eddy correlation method and averaged over 2-min intervals. Ogive curves were examined to select the averaging interval that, if longer, would provide little change to the flux values.

Although sampling limitations prevent the calculation of an average map of the stresses from all flight legs, the location of the highest stress values (greater than two standard deviations above the mean from the 30-m legs) were recorded along northern California and the lee of Point Sur, where the COAMPS stresses are high. The distribution of all aircraft stress measurements (Fig. 11) shows magnitudes similar to those calculated in the COAMPS average.

The EC-130Q aircraft flights provide directly measured examples along west coast capes under northerly flow (Fig. 12). Each is a map of all low-level aircraft stress measurements at a nominal 30-m flight elevation taken on that day. At Cape Blanco (1 July, Fig. 12a), Cape Mendocino (12 June, Fig. 12b), and Point Sur (17 June, Fig. 12c) stress was lower on the north side of the cape and greatly increased in the lee. The greatest wind stress is 0.56 N m^{-2} in the lee of Cape Mendocino. All of these cases have a supercritical MABL upstream of the cape (Fig. 7) and fit the criteria for a supercritical expansion fan in the lee (as defined in Dorman et al. 1999). For the north side of Point Conception (29 June, Fig. 12d), the stress is much greater offshore than close to the coast.

Similar wind stress values and structures under northerly flow were found at Point Arena (Enriquez and Friehe 1995). Aircraft mapping around five capes in two field projects shows that there can be an enormous variation of the surface wind stress on a small scale (10 km) around major capes. Magnitudes can vary over this scale, compromising stress estimates based upon isolated buoys or remote systems with footprints greater than the order of 10 km.

b. COAMPS

Sea surface wind stress forces the upper ocean (Gill 1982) and affects a number of physical and biological processes in the ocean (Brink et al. 1992; U.S. GLOBEC 1994). In the past, it has been difficult to determine the detailed structure of the surface stress because of the dearth of direct measurements and uncertainties in mod-

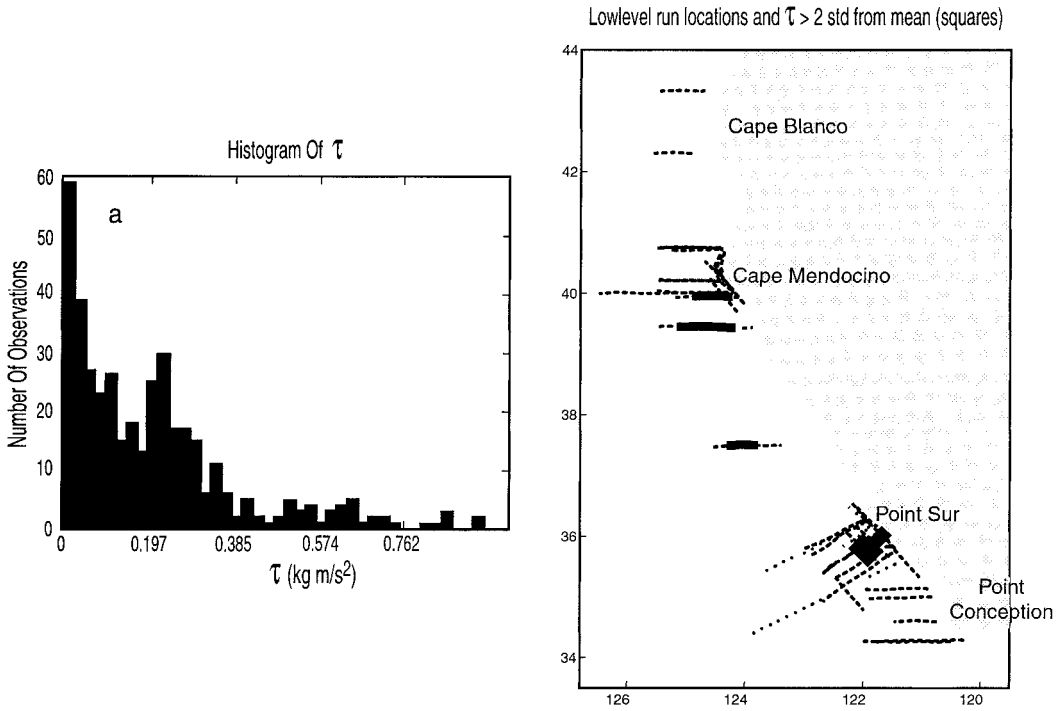

FIG. 11. Statistics of Jun 1996 aircraft stress measurements. (left) Distribution. (right) Thick lines are flight tracks with stresses >2 standard deviations of the mean of all flights and light lines are less.

eling. Further, limited coastal measurements have shown that there can be great structure in the coastal winds, which implies great structure in the surface wind stress. The ability of high-resolution mesoscale models to capture the details of the coastal wind field has encouraged us to compute the wind stress from COAMPS.

The COAMPS model sea surface wind stress uses the model's 10-m winds and the sea surface and 2-m temperatures. The result is a broad, alongcoast maximum with values exceeding 0.3 N m^{-2} north of San Francisco and the peak in the lee of Cape Mendocino (Fig. 13). Isolated and lower-valued peaks are downwind of Points Sur and Conception.

No observations of the stress exist on a space and time scale comparable to the COAMPS 2-month average. However, the stress calculated by the model is consistent with the median values of the aircraft stresses for June–July 1996. The model's stress structure is consistent with the aircraft within the limitations of the aircraft sampling, as both have the highest values nearshore and along the northern California coast and with local maximums in the lee of every major cape. Local stress minima are found on the upwind side of every cape, with the absolute minimum in the southern California Bight.

6. Discussion

Few observations are available with the geographic and time coverage of the COAMPS June–July averaged outputs, yet such a comparison is desirable. Three remotely sensed fields were compared to the COAMPS model results: wind speed, the cloud cover (a rough proxy of MABL height), and SST.

a. SSM/I wind speeds

The 10-m wind speed over the ocean can be derived from SSM/I observations. We include this here as an estimate of the overwater conditions on a scale comparable to COAMPS, although we do not consider it to be as reliable and accurate as direct measurements. SSM/I is a passive microwave radiometer carried aboard several Defense Meteorological Satellite Program satellites that detects the brightness temperature of the ocean. An algorithm developed by Wentz (1997) translates this temperature into the surface wind speed. The resulting wind speed fields at 25-km resolution were obtained from Remote Sensing Systems, Santa Rosa, California. To avoid mixing land and sea grid points, only observations greater than 50 km from the coast are used. The morning and evening passes with the best coverage of the region were selected for each day of June and July 1996 and averaged (Fig. 14).

There are two broad speed maxima, one off northern California and one off southern California. The broad offshore maxima corresponds to the magnitude and area for the COAMPS wind field (Fig. 8a). Although the distributions differ, especially to the south, the differences are not necessarily significant since wind fields

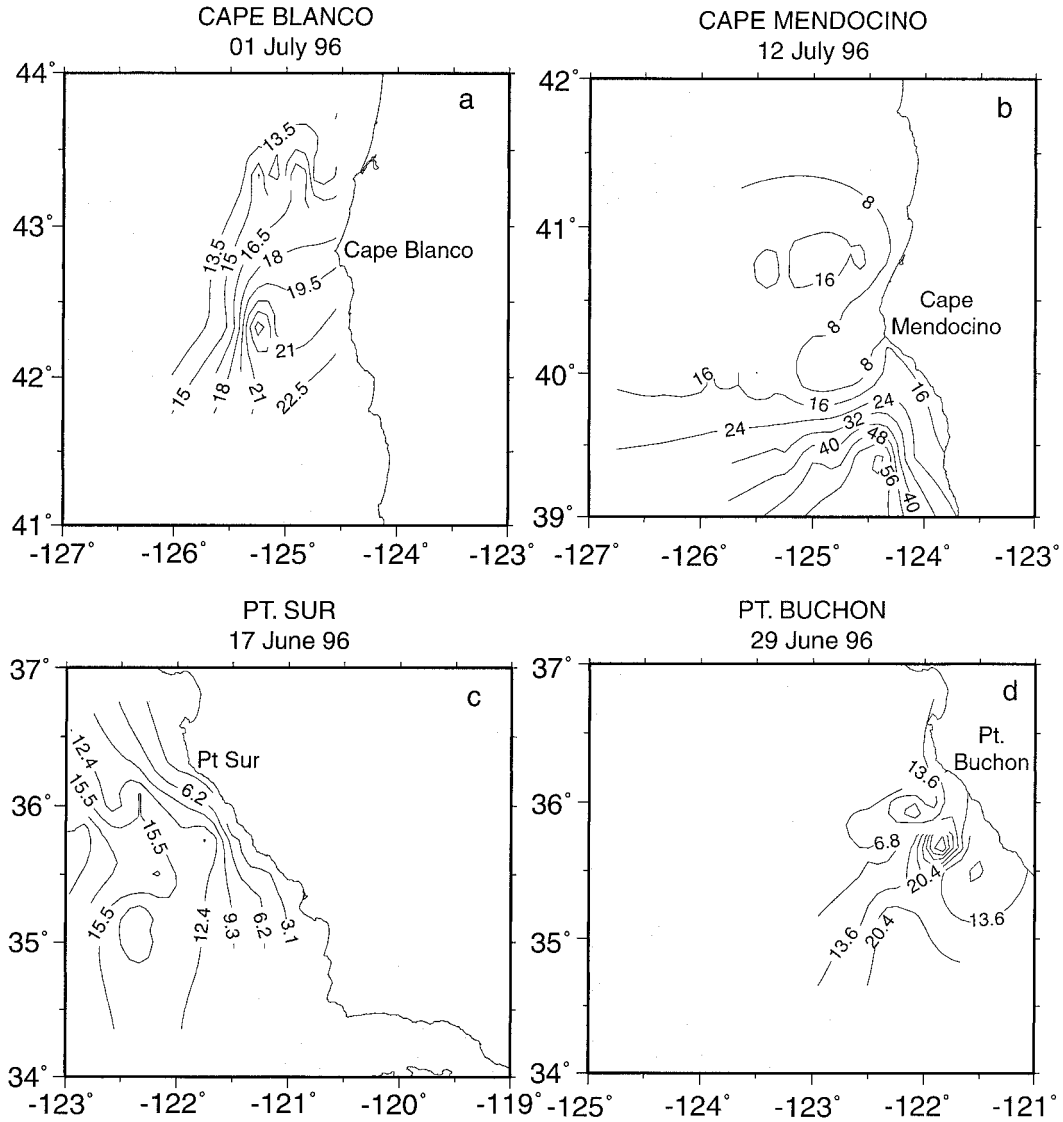

FIG. 12. Aircraft stress maps (N $m^{-2} \times 100$) corresponding to the maps in Figs. 5, 6, and 7.

from the individual satellite passes are noisy and the error in the SSM/I wind speed is suggested to be of the order of ± 1 m s^{-1}. In summary, a broad 10-m wind speed maxima extending along California for June–July 1996 is supported by the SSM/I and COAMPS analysis.

b. Cloud cover

A second data set from which a June–July average could be constructed with similar spatial coverage to COAMPS was remotely sensed cloud cover, which is a rough proxy of MABL height. Summer clouds over the ocean in this area are mostly stratus that are restricted to the MABL. The amount of the stratus tends to increase with the MABL depth (Rosenthal 1972; Dorman 1985). To examine the cloud structure, the albedo of *Geostationary Operational Environmental Satellite-9* (*GOES-9*) visual images were averaged by hour for June–July 1996. The result shown in Fig. 15 is the percent albedo such that 100 would represent a cloud overcast for 100% of all observations at a point. As there is a generally decreasing trend in cloud cover after sunrise, the 1200 PST average is presented, which is typical of the daylight mean. Nighttime estimates of low marine clouds based upon the infrared sensors are less certain since the marine cloud-top temperatures are close to the sea surface temperatures, making the two difficult to distinguish.

Beyond 100 km from the coast, the marine cloud cover increases from about 39°N (Point Arena) to the south, with the thickest clouds off southern California. North of Cape Mendocino, there tends to be an inner coastal zone 50–100 km wide of marine clouds with more opaque, smoother tops than those farther offshore.

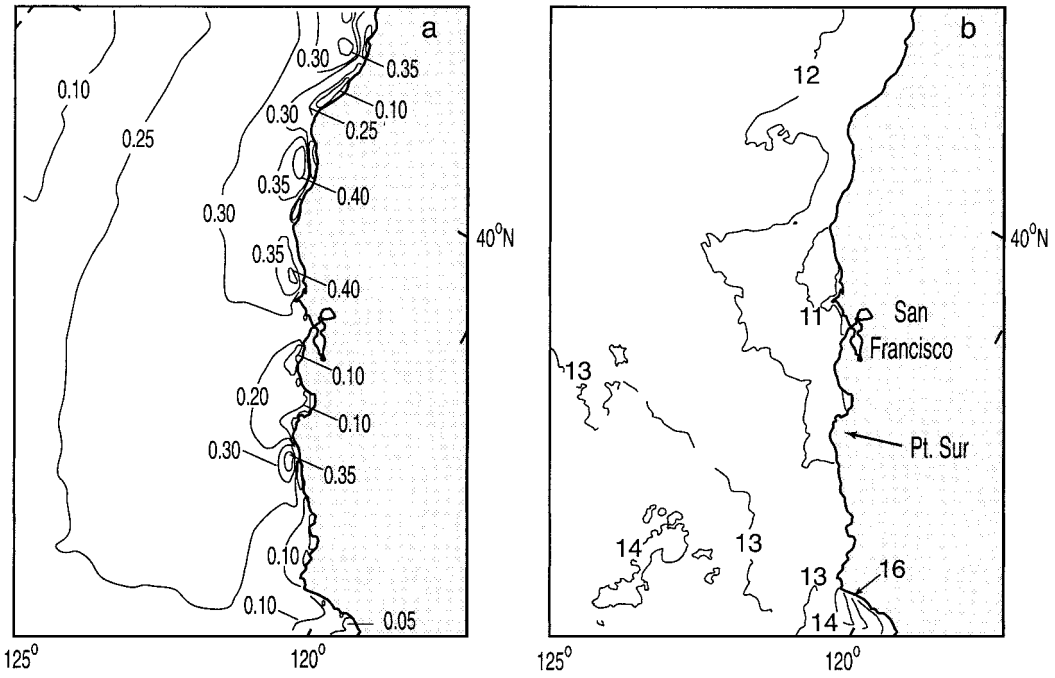

FIG. 13. (a) COAMPS sea surface wind stress (N m^{-2}). (b) Sea surface temperatures adapted from infrared satellite images averaged for Jun–Jul 1996.

There are distinct clear patches in the lee of prominent coastal topography at all major West Coast capes. These are especially apparent for Cape Mendocino, Point Arena, Point Sur, and Point Conception. As the daylight hour increases, the albedo decreases in the lee and the offshore extent of the clear patch increases. These lee clearings are consistent with expansion fans in the lee of capes, which produce a locally thin MABL that thins further as the MABL speeds increase during the solar day. In contrast, the weak coastal wind zone in the eastern and southern portions of the southern California Bight shows diurnal clearing associated with local heating effects.

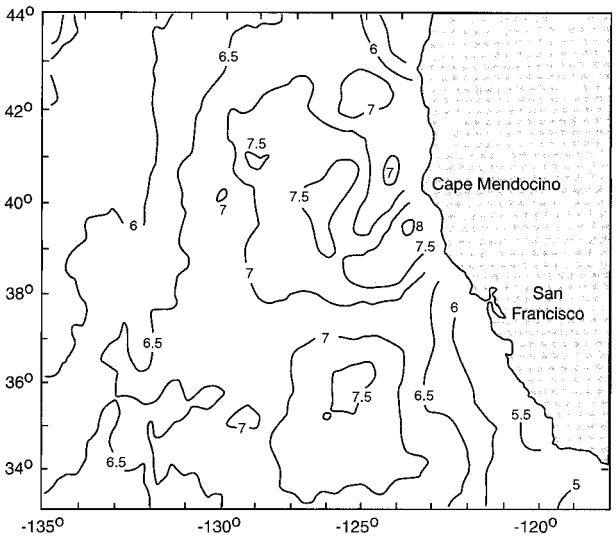

FIG. 14. SSM/I 10-m wind speeds averaged over Jun–Jul 1996 (m s^{-1}).

The topographically forced cloud features are robust, appearing frequently on individual satellite images as on the GOES image at 1330 PST on 23 June 1996 (Fig. 16). Also superimposed on Fig. 16 are the air temperature inversion base height (m) determined by aircraft soundings between 1200 and 1700 PST on the same day. Abrupt clearing occurs at the edges of the four coastal inversion base minima in this scene: to the north of Point Sur over Monterey Bay, on the south edge of Point Sur, just to the northwest of Point Conception, and to the east of Point Conception. Between the first two and second two minima are narrow ridges of inversion base maxima outlined by opaque cloud cover. Aircraft soundings around clouds on other days in June and July 1996 confirm that cloud cover tends to decrease with lower MABL heights.

COAMPS June–July averaged fields of cloud liquid water forecast using the Rutledge–Hobbs explicit moist physics are shown in Fig. 17. The field represents a vertically weighted average of cloud water (g kg^{-1}) throughout the model column. The maxima along the coast south of San Francisco Bay are due to low-level ($<$450 m) clouds while the maxima offshore is at higher levels ($<$750 m), reflecting the sloping marine inversion. The distinct clear patches in the lee of major West Coast capes are prominent as in the observations (Fig. 15). The observed inner coastal zone maxima north of

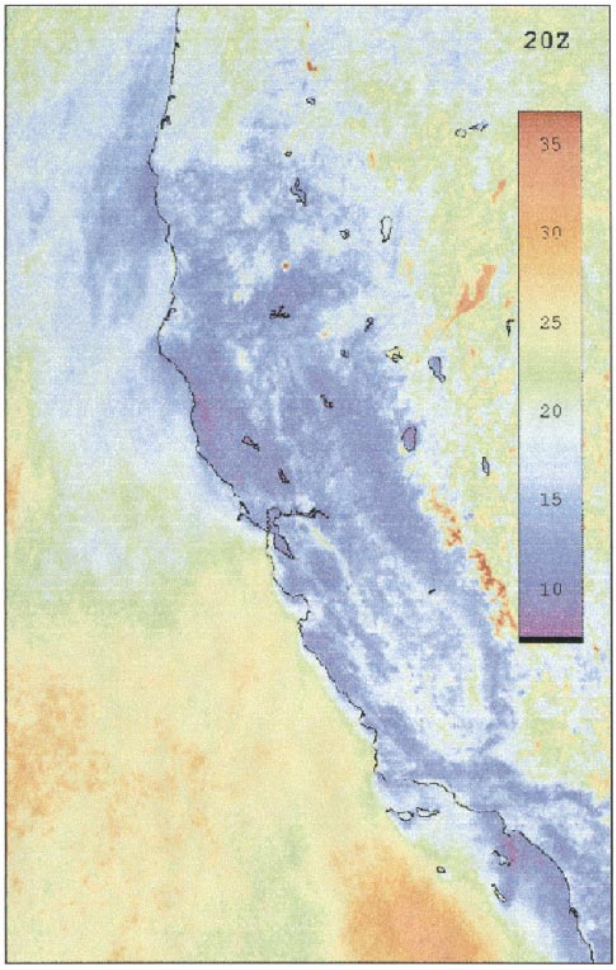

FIG. 15. Mean cloud cover in percent for Jun–Jul 1996 from the *GOES-9* visible band at 1200 PST.

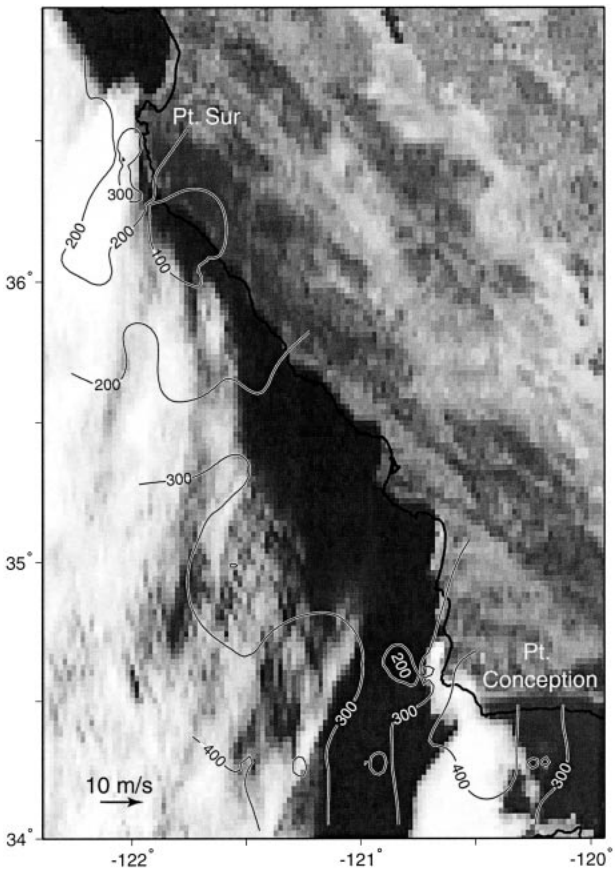

FIG. 16. *GOES-9* visible band clouds for 1330 PST 23 Jun 1996. Contours are the air temperature inversion base height (m) measured by aircraft soundings between 1200 and 1700 PST.

Cape Mendocino, though hinted at in the model average, is not as evident as the coastal maxima to the south.

c. Sea surface temperature

The third large-scale observation to compare to the COAMPS model average fields is the June–July sea surface temperature field (Fig. 13b) from Advanced Very High Resolution Radiometer satellite observations. The SST distribution is similar to that of the COAMPS model wind stress (Fig. 13a). Coldest waters are found along the northern California coast between San Francisco and the lee of Cape Blanco. The 12° isotherm from the satellite observations extends alongshore in a similar pattern to the model's 0.3 N m^{-2} isoline. It appears that simple wind stress could explain these major features of the sea surface temperature field along California during the summer. Farther south, however, the wind speed maximum off central California and Point Conception does not translate into high wind stress in the model results, nor into cool water temperatures.

d. MABL Froude number

We were interested in computing the MABL Froude number from the coastal sounding stations that have long temporal records and might be used to check on the June–July 1996 averaged model values. The NOAA/ETL radar profilers observe the hourly wind and virtual temperature profiles, allowing the Froude number to be computed by the same technique that was used for the aircraft values (section 3c). Unfortunately, the coastal profiler data appear to systematically underrepresent the Froude number over the water. Typical results are presented in Table 5, which gives the Froude number at selected sites along the coast. To verify the radar data against the in situ measurements, the profiler observation closest in time to nearby aircraft profiles was selected. Data from the two closest aircraft profiles were averaged and used to compute the aircraft based Froude number.

With the exception of the Point Arena profiler, the Froude numbers from the aircraft profiles are about

twice as high as the Froude number from the radar profilers. The difference is due to the fact that the layer-averaged speeds are faster over water than land. Wind speeds over water typically increase vertically from the surface to the base of the air temperature inversion, and remain fast well into the air temperature inversion. On the other hand, the land speed profiles are significantly different even if only 100 m inland. The land drag slows the mean speed throughout the whole MABL. Above the base of the air temperature inversion, speeds fall off immediately, further lowering the vertically averaged mean, since MABL height is defined as the middle of the inversion. The result is that land-based Froude numbers are in the lower subcritical range while nearby overwater values can be supercritical over an extensive area.

The difference in land and overwater speeds is apparent in the June–July means. The Froude numbers based upon the profiler averages are all in the low subcritical range, except for Point Arena. However, the COAMPS model Froude number field suggests that most of the overwater coastal Froude numbers are either close to or are supercritical. The conclusion is that land-based soundings should not be used to compute the overwater Froude number.

7. Conclusions

Fixed coastal surface and sounding stations and aircraft mapping flights within 100–120 km of major capes were combined to record the large-scale features of the MABL along Oregon and California in summer 1996. These observations were extended offshore by the U.S. Navy's COAMPS mesoscale model.

Coastal measurements and numerical modeling support the existence of a broad, high speed surface wind pattern along the California coast in summer. Near the coast, wind speeds peak along northern California with a higher peak near Point Conception. This is somewhat different from ship-based wind analyses that support only a single peak along northern California (Nelson 1977; Nelson and Husby 1983). Measurements presented here show that mean wind speeds are greater at buoys 15–25 km offshore than at nearby land stations. The winds from the coastal stations are fastest in the afternoon, but are lower than the mean speed at the nearest buoy. Therefore coastally measured winds will in most cases be an underestimate of the wind speeds just offshore.

The aircraft data and model show that an air temperature inversion caps the MABL with a base that is lowest at the coast and deeper offshore. Along the coast there is a broad minimum in MABL height between Cape Blanco and Santa Barbara. The inversion base height is an absolute low in northern California (below 200 m at Bodega Bay) and is substantially higher at Los Angeles and San Diego (above 400 m).

The MABL is typically supercritical (Froude number > 1) in a region that extends from northern Monterey Bay to Cape Mendocino and to 150 km offshore based upon COAMPS and supported by aircraft data. Isolated supercritical or enhanced supercritical regions are found on the south side of every major cape, with the largest region in the lee of Cape Mendocino and smaller regions downwind of capes to the south. A broad wedge-shaped area of nearly critical flow (Froude number > 0.8) extends alongcoast from Cape Blanco to Point Piedras Blancas and offshore to 200 km in the June–July COAMPS average. This region could be supercritical during a significant portion of the averaging period.

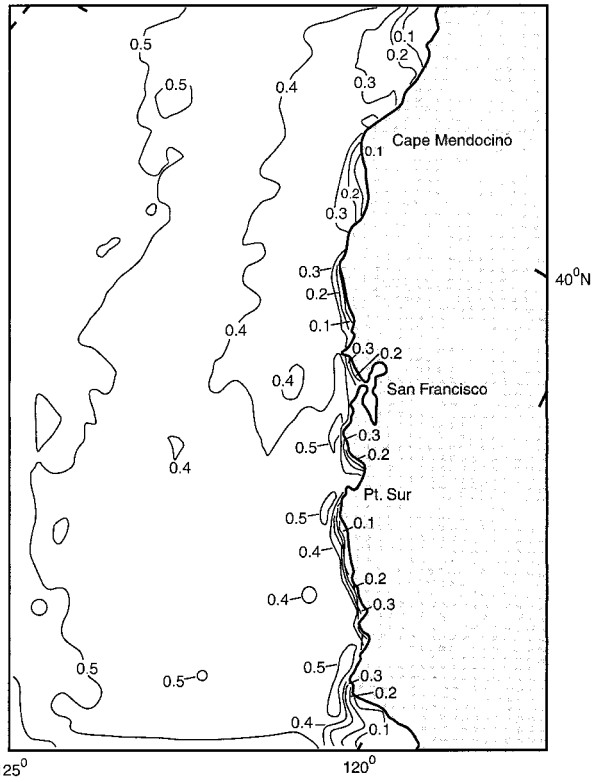

FIG. 17. COAMPS vertically averaged MABL cloud liquid water (g kg^{-1}).

The large-scale, sea surface wind stress is largest between Cape Mendocino and San Francisco and within 100 km of the coast. The stress is lower near the coast of central California just to the north of Point Conception. The high stress region corresponds to an area of cold sea surface temperatures, consistent with local wind-driven upwelling. In the small scale, aircraft measurements show wind stress extrema in the vicinity of all major capes sampled under northerly flow.

Acknowledgments. Support was provided by the Office of Naval Research and the National Science Foundation Division of Atmospheric Sciences. COAMPS simulations were performed at the Fleet Numerical Modeling and Oceanography Center Cray C90. The ma-

TABLE 5. Froude numbers from aircraft and profilers.

Instantaneous values	H (m)	C (m s^{-1})	$\theta_\mu - \theta$ (K)	θ (K)	Froude
Cape Blanco					
Aircraft profile	361	15.2	5	287	1.88
Profiler NPT	445	8.3	5	287	0.92
Buoy 50		6.5			
Aircraft profile	341	18.4	7	288	2.03
Profiler CRC	360	5.6	10	288	0.52
Buoy 27		7.6			
Cape Mendocino					
Aircraft profile	475	18.3	10	285	1.41
Profiler PAA	378	12.2	4	282	1.80
Buoy 14		7.9			
Point Sur					
Aircraft profile	404	15.6	4	284	2.05
Profiler FTO	483	8.0	6	284	0.79
Buoy 42		11.4			
Aircraft profile	397	18.3	7	287	1.87
Profiler PPB	375	9.5	9	286	0.90
Buoy 28		14.9			
Point Conception					
Aircraft profile	208	9.7	7	294	1.40
Profiler GLA	286	3.4	2	301	0.73
Buoy 51		6.6			
Jun–Jul 1996 Avg					
Profiler NPT	586	6.7	8	287	0.62
Buoy 50		3.7			
Profiler CRC	516	5.0	9	286	0.48
Buoy 27		4.2			
Profiler PAA	446	9.7	9	285	1.03
Buoy 14		6.3			
Profiler FTO	709	3.2	12	284	0.24
Buoy 42		5.5			
Profiler PPB	616	3.3	12	286	0.26
Buoy 28		7.4			
Profiler GLA	643	2.5	10	288	0.20
Buoy 51		6.6			

jority of the sounding data was from the network maintained by NOAA/ERL/Environmental Technology Laboratory, Boulder. We are grateful for the aggressive and inspired data retrieval and salvage by Dick Lind at the Naval Postgraduate School.

REFERENCES

Baker, N. L., 1992: Quality control for the U.S. Navy operational database. *Wea. Forecasting,* **7,** 250–261.

Beardsley, R. C., C. E. Dorman, C. A. Friehe, L. K. Rosenfeld, and C. D. Winant, 1987: Local atmospheric forcing during the Coastal Ocean Dynamics Experiment. 1. A description of the marine boundary layer and atmospheric conditions over a northern California upwelling region. *J. Geophys. Res.,* **92,** 1467–1488.

Bridger, A. F. C., W. C. Brick, and P. F. Lester, 1993: The structure of the marine inversion layer off the central California coast. *Mon. Wea. Rev.,* **121,** 335–351.

Brink, K. H., and Coauthors, 1992: Coastal ocean processes: A science prospectus. Woods Hole Oceanographic Institution Tech. Rep. WHOI-92-18, 70 pp. [Available from WHOI, Woods Hole, MA 02543-1541.]

Brost, R. A., D. H. Lenshow, and J. C. Wyngaard, 1982a: Marine stratocumulus layers. Part I: Mean conditions. *J. Atmos. Sci.,* **39,** 800–817.

——, J. C. Wyngaard, and D. H. Lenshow, 1982b: Marine stratocumulus layers. Part II: Turbulence budgets. *J. Atmos. Sci.,* **39,** 818–835.

Burk, S. D., and W. T. Thompson, 1996: The summertime low-level jet and marine boundary layer structure along the California coast. *Mon. Wea. Rev.,* **124,** 668–686.

——, T. Haack, and R. M. Samelson, 1999: Mesoscale simulation of supercritical, subcritical, and transcritical flow along coastal topography. *J. Atmos. Sci.,* **56,** 2780–2795.

Cui, Z., M. Tjernstrom, and B. Grisogono, 1998: Idealized simulations of atmospheric coastal flow along the central coast of California. *J. Appl. Meteor.,* **37,** 1332–1363.

Dorman, C. E., 1982: Winds between San Diego and San Clemente Island. *J. Geophys. Res.,* **87,** 936–946.

——, 1985: Evidence of Kelvin waves in California's marine layer and related eddy generation. *Mon. Wea. Rev.,* **113,** 827–839.

——, and C. D. Winant, 1995: Buoy observations of the atmosphere along the west coast of the United States, 1981–1990. *J. Geophys. Res.,* **100,** 16 029–16 044.

——, and ——, 2000: The structure and variability of the marine atmosphere around the Santa Barbara Channel. *Mon. Wea. Rev.,* **128,** 261–282.

——, D. P. Rogers, W. Nuss, and W. T. Thompson, 1999: Adjustment of the summer marine boundary layer around Point Sur, California. *Mon. Wea. Rev.,* **127,** 2143–2159.

Doyle, J. D., 1997: The influence of mesoscale orography on a coastal jet and rainband. *Mon. Wea. Rev.,* **125,** 1465–1488.

Enriquez, A. G., and C. A. Friehe, 1995: Effects of wind stress and wind stress curl variability on coastal upwelling. *J. Phys. Oceanogr.,* **25,** 1651–1671.

——, and ——, 1997: Bulk parameterization of momentum, heat, and moisture fluxes over a coastal upwelling area. *J. Geophys. Res.,* **102,** 5781–5798.

Gal-Chen, T., and R. C. J. Somerville, 1975: On the use of a coordinate-transformation for the solution of the Navier–Stokes equations. *J. Comput. Phys.,* **17,** 209–228.

Gill, A. E., 1982: *Atmosphere–Ocean Dynamics.* Academic Press, 662 pp.

Haack, T., and R. M. Hodur, 1997: A coupled ocean/atmospheric modeling study of an arctic lead. *The Air-Sea Interface Radio and Acoustic Sensing, Turbulence and Wave Dynamics,* M. A. Donelan, W. H. Hui, and W. J. Plant, Eds., Rosenstiel School of Meteorology and Oceanography, University of Miami, 579–586.

Halliwell, G. R., and J. S. Allen, 1987: The large-scale coastal wind field along the west coast of North America. *J. Geophys. Res.,* **92,** 1497–1506.

Hamilton, G. D., 1980: NOAA data buoy office programs. *Bull. Amer. Meteor. Soc.,* **61,** 1012–1017.

Harshvardhan, R. Davies, D. Randall, and T. Corseti, 1987: A fast radiation parameterization for atmospheric circulation models. *J. Geophys. Res.,* **92,** 1009–1015.

Henderson, F. M., 1966: *Open Channel Flow.* Macmillan, 522 pp.

Hodur, R., 1997: The Naval Research Laboratory's Coupled Ocean/Atmosphere Mesoscale Prediction System (COAMPS). *Mon. Wea. Rev.,* **125,** 1414–1430.

——, L. R. Brody, R. Englebretson, T. Holt, S. Lowe, C. Wash, and L. Zambresky, 1996: Validation test report for the Coupled Ocean/Atmosphere Mesoscale Prediction System (COAMPS). NRL Internal Rep., 50 pp. [Available from Librarian, Naval Research Laboratory, Monterey, CA 93943.]

Holt, T. R., 1996: Mesoscale forcing of a boundary layer jet along the California coast. *J. Geophys. Res.,* **101,** 4235–4254.

Junker, N. W., J. E. Hoke, and R. H. Grumm, 1989: Performance of NMC's regional models. *Wea. Forecasting,* **4,** 368–390.

Kain, J. S., and J. M. Fritsch, 1990: A one-dimensional entraining/detraining plume model and its application in convective parameterization. *J. Atmos. Sci.,* **47,** 2784–2802.

Louis, J. F., M. Tiedtke, and J. F. Geleyn, 1982: A short history of

the operational PBL parameterization at ECMWF. *Workshop on Planetary Boundary Parameterization*, Reading, United Kingdom, ECMWF, 59–79.

Neiburger, M., D. S. Johnson, and C. Chien, 1961: Studies of the structure of the atmosphere over the eastern Pacific Ocean in summer, I, The inversion over the eastern North Pacific Ocean. *Univ. Calif. Publ. Meteor.*, **1,** 1–99.

Nelson, C. S., 1977: Wind stress and wind stress curl over the California Current. NOAA Tech. Rep. NMFS SSRF-714, 87 pp. [NTIS PB-273610.]

——, and D. M. Husby, 1983: Climatology of surface heat fluxes over the California Current region. NOAA Tech. Rep. NMFS SSRF-763, 155 pp. [Available from National Marine Fisheries Service, 7600 Sand Point Way, Seattle, WA 98115-0070.]

Petterssen, S., 1956: *Weather Analysis and Forecasting.* Vol. I. McGraw-Hill, 428 pp.

Ralph, F. M., L. Armi, J. M. Bane, C. E. Dorman, W. D. Neff, P. J. Neiman, W. Nuss, and P. O. G. Persson, 1998: Observations and analysis of the 10–11 June 1994 coastally trapped disturbance. *Mon. Wea. Rev.*, **126,** 2435–2465.

Robinson, M. K., 1976: *Atlas of North Pacific Ocean Monthly Mean Temperatures and Mean Salinities of the Surface Layer*. NOO RP-2, 194 pp. [Available from Naval Oceanographic Office, Washington, DC 20373.]

Rogers, D., and Coauthors, 1998: Highlights of Coastal Waves 1996. *Bull. Amer. Meteor. Soc.*, **79,** 1307–1326.

Rogerson, A. M., 1999: Transcritical flows in the coastal marine atmospheric boundary layer. *J. Atmos. Sci.*, **56,** 2761–2779.

Rosenthal, J., 1972: Point Mugu forecasters handbook. Pacific Missel Range Tech. Publ. PMR-TP-72-1, 278 pp. [Available from Pacific Missle Range, Pt. Mugu, CA 93042-5000.]

Rotunno, R., and Coauthors, 1992: *Coastal Meteorology. A Review of the State of the Science.* National Academy Press, 99 pp.

Rutledge, S. A., and P. V. Hobbs, 1983: The mesoscale and microscale structure of organization of clouds and precipitation in midlatitude cyclones. VIII: A model for the ''seeder-feeder'' process in warm-frontal rainbands. *J. Atmos. Sci.*, **40,** 1185–1206.

Samelson, R. M., 1992: Supercritical marine-layer flow along a smoothly varying coastline. *J. Atmos. Sci.*, **49,** 1571–1584.

Therry, G., and P. LaCarrere, 1983: Improving the eddy kinetic energy model for planetary boundary layer description. *Bound.-Layer Meteor.*, **25,** 63–88.

Thompson, W. T., T. Haack, J. D. Doyle, and S. D. Burk, 1997: A nonhydrostatic mesoscale simulation of the 10–11 June 1994 coastally trapped wind reversal. *Mon. Wea. Rev.*, **125,** 3211–3230.

U.S. GLOBEC, 1994: Eastern boundary Current Program. Rep. 11, 99 pp. [Available from U.S. Global Ocean Ecosystems, Dynamics, University of California, Berkeley, CA 94720-3140.]

Wentz, F. J., 1997: A well-calibrated ocean algorithm for Special Sensor Microwave/Imager. *J. Geophys. Res.*, **102,** 8703–8718.

Winant, C., C. Dorman, C. Friehe, and R. Beardsley, 1988: The marine layer off northern California: An example of supercritical channel flow. *J. Atmos. Sci.*, **45,** 3588–3605.

Zemba, J., and C. A. Friehe, 1987: The marine atmospheric boundary layer jet in the Coastal Ocean Dynamics Experiment. *J. Geophys. Res.*, **92,** 1489–1496.